

Mechanical stress relief in porous silicon free standing membranes

Romain Guider,^{1,*} Cristina Traversa¹ and Paolo Bettotti¹

¹ Nanoscience Laboratory, Department of Physics, University of Trento, Via Sommarive 14, 38123 Povo (TN), Italy
*romain.guider@unitn.it

Abstract: In this work, we report on the difference of mechanical stress in free standing and attached Porous silicon membranes. By performing Raman analysis, we demonstrate that the tensile stress accumulated during the etching process by the porous silicon layer is partially compensated by the presence of the substrate. We highlight this complex effect by experimentally showing the balancing effect of the substrate and the change in mechanical stress between top and bottom surfaces in free standing membranes. In addition, this Raman investigation allows us to separate the effects on the Raman lineshape due to the nanostructures from those related with the mechanical stress of macroscopic structures.

©2015 Optical Society of America

OCIS codes: (300.6450) Spectroscopy, Raman; (310.4925) Other properties (stress, chemical, etc.); (240.6490) Spectroscopy, surface.

References and links

1. N. Kumar, E. Froner, R. Guider, M. Scarpa, and P. Bettotti, "Investigation of non-specific signals in nanoporous flow-through and flow-over based sensors," *Analyst (Lond.)* **139**(6), 1345–1349 (2014).
2. J. de Boor, D. S. Kim, X. Ao, D. Hagen, A. Cojocaru, H. Foll, and V. Schmidt, "Temperature and structure size dependence of the thermal conductivity of porous silicon," *EPL* **96**(1), 16001 (2011).
3. F. Haase, S. Kajari-Schröder, and R. Brendel, "High efficiency back-contact back-junction thin-film monocrystalline silicon solar cells from the porous silicon process," *J. Appl. Phys.* **114**(19), 194505 (2013).
4. M. Ghulinyan, C. J. Oton, Z. Gaburro, P. Bettotti, and L. Pavesi, "Porous silicon free-standing coupled microcavities," *Appl. Phys. Lett.* **82**(10), 1550–1552 (2003).
5. P. Bettotti, L. Dal Negro, Z. Gaburro, L. Pavesi, A. Lui, M. Galli, M. Patrini, and F. Marabelli, "P-type macroporous silicon for two-dimensional photonic crystals," *J. Appl. Phys.* **92**(12), 6966–6972 (2002).
6. Md. N. Islam and S. Kumar, "Influence of crystallite size distribution on the micro-Raman analysis of porous Si," *Appl. Phys. Lett.* **78**(6), 715–717 (2001).
7. D. Papadimitriou, J. Bitsakis, J. M. Lopez-Villegas, J. Samitier, and J. R. Morante, "Depth dependence of stress and porosity in porous silicon: a micro-Raman study," *Thin Solid Films* **349**(1), 293–297 (1999).
8. M. Yang, D. Huang, P. Hao, F. Zhang, X. Hou, and X. Wang, "Study of the Raman peak shift and the linewidth of light-emitting porous silicon," *J. Appl. Phys.* **75**(1), 651–653 (1994).
9. I. H. Campbell and P. M. Fauchet, "The effects of microcrystal size and shape on the one phonon Raman spectra of crystalline semiconductors," *Solid State Commun.* **58**(10), 739–741 (1986).
10. V. Paillard, P. Puech, R. Sirvin, S. Hama, and P. Roca i Cabarrocas, "Measurement of the in-depth stress profile in hydrogenated microcrystalline silicon thin films using Raman spectrometry," *J. Appl. Phys.* **90**(7), 3276–3279 (2001).
11. Y. Kanemitsu, H. Uto, Y. Masumoto, T. Matsumoto, T. Futagi, and H. Mimura, "Microstructure and optical properties of free-standing porous silicon films: Size dependence of absorption spectra in Si nanometer-sized crystallites," *Phys. Rev. B Condens. Matter* **48**(4), 2827–2830 (1993).
12. D. Abidi, B. Jusserand, and J.-L. Fave, "Raman scattering studies of heavily doped microcrystalline porous silicon and porous silicon free-standing membranes," *Phys. Rev. B* **82**(7), 075210 (2010).
13. H. Tanino, A. Kuprin, H. Deai, and N. Koshida, "Raman study of free-standing porous silicon," *Phys. Rev. B Condens. Matter* **53**(4), 1937–1947 (1996).
14. Q. Li, W. Qiu, H. Tan, J. Guo, and Y. Kang, "Micro-Raman spectroscopy stress measurement method for porous silicon film," *Opt. Lasers Eng.* **48**(11), 1119–1125 (2010).
15. A. Martínez, J. Blasco, P. Sanchis, J. V. Galán, J. García-Rupérez, E. Jordana, P. Gautier, Y. Lebour, S. Hernández, R. Guider, N. Dalbosco, B. Garrido, J. M. Fedeli, L. Pavesi, J. Martí, and R. Spano, "Ultrafast all-Optical Switching in a Silicon-Nanocrystal-Based Silicon Slot Waveguide at Telecom Wavelengths," *Nano Lett.* **10**(4), 1506–1511 (2010).

16. M. Cazzanelli, F. Bianco, E. Borgia, G. Pucker, M. Ghulinyan, E. Degoli, E. Luppi, V. Véniard, S. Ossicini, D. Modotto, S. Wabnitz, R. Pierobon, and L. Pavesi, "Second-harmonic generation in silicon waveguides strained by silicon nitride," *Nat. Mater.* **11**(2), 148–154 (2011).
17. N. Kumar, S. Gennaro, P. Sasikumar, G. D. Sorarù, and P. Bettotti, "Self detachment of free-standing porous silicon membranes in moderately doped n-type silicon," *Appl. Phys., A Mater. Sci. Process.* **116**(1), 251–257 (2014).
18. P. C. Ricci, R. Casula, G. Gulleri, F. Fumagalli, C. M. Carbonaro, and R. Corpino, "Mechanical stress in silicon nanosized architectures: Defects of SOD processed silica filler," *J. Alloys Compd.* **602**, 157–162 (2014).
19. S. Manotas, F. Agullo-Rueda, J. D. Moreno, F. Ben-Hander, R. Guerrero-Lemus, and J. M. Martinez-Duart, "Laser heating in porous silicon studied by micro-Raman spectroscopy," *Phys. Status Solidi* **182**(1), 331–334 (2000).
20. I. De Wolf, "Micro-Raman spectroscopy to study local mechanical stress in silicon integrated circuits," *Semicond. Sci. Technol.* **11**(2), 139–154 (1996).
21. M. A. Green, "Self-consistent optical parameters of intrinsic silicon at 300 K including temperature coefficients," *Sol. Energy Mater. Sol. Cells* **92**(11), 1305–1310 (2008).
22. N. Kumar, "Fabrication of n-type porous silicon membranes for sensing applications," PhD Thesis, University of Trento, Trento, Italy, 2013, <http://eprints-phd.biblio.unitn.it/1127/1/thesis.pdf>
23. I. Avrutsky, R. Gibson, J. Sears, G. Khitrova, H. M. Gibbs, and J. Hendrickson, "Linear systems approach to describing and classifying Fano resonances," *Phys. Rev. B* **87**(12), 125118 (2013).
24. <http://www.mathworks.com/matlabcentral/fileexchange/24916-baseline-fit>
25. F. Cerdeira, C. J. Buchenauer, F. H. Pollak, and M. Cardona, "Stress-Induced Shifts of First-Order Raman Frequencies of Diamond- and Zinc-Blende-Type Semiconductors," *Phys. Rev. B* **5**(2), 580–593 (1972).
26. Z. Iqbal and S. Veprek, "Raman scattering from hydrogenated microcrystalline and amorphous silicon," *J. Phys. C Solid State Phys.* **15**(2), 377–392 (1982).

1. Introduction

Porous silicon (PSi) has been investigated for decades for its peculiar optical and structural properties and the interest is far from fading out as demonstrated by its recent uses as sensor [1], thermoelectric [2] and photovoltaic device [3]. Despite its fascinating properties, the use of PSi in real products is still hampered by the limited reproducibility assured by the electrochemical etching. The main reason is the very high sensitivity of the etching towards experimental details (such as: Si wafer type, geometry of the electrochemical cell and of the electrode, etc.).

An interesting characteristic of PSi is the possibility to detach the porous layer from the substrate with a sudden increase of the current at the end of the etching [4] and to create free standing membranes (FSM). The highly anisotropic structure of the PSi's pores permits to exploit FSMs as hosts for optical (bio)sensors as well as filtering systems. Currently one of the main limitations to fully exploit nano-PSi capabilities is the fabrication of thick and mechanically robust FSMs. In fact, while it is rather easier to obtain thin films, membranes thicker than several tens of microns are difficult to handle as they tend to roll-up and crack because of mechanical stress accumulated during the etching. This fact is due to a porosity gradient that develops during the etching and that limits the maximum anisotropy and aspect ratio attainable with the electrochemical method, due to the enlargement of the pore dimensions along the etching process [5].

Several papers already reported Raman analysis on PSi and describe how the main parameters are connected with the structure of the PSi skeleton either in terms of crystallite size [6] or of mechanical stress [7, 8]. Unfortunately the Raman response is the result of the interplay among quantum size and mechanical effects [9] and their response can be separated only by using independent characterization techniques [10]. Among the few articles which analyze FSMs [11–13], none of them compare free standing and supported samples obtained using the same etching conditions.

In [14] the authors report a comprehensive model of the stress in PSi layers (PSL). Confocal Raman mapping is used to analyze the stress profile in both PSi and the underlying crystalline substrate. The authors correctly notice that the stress induced by the porosification of the semiconductor might produce a bending of the whole structure. This fact is well shown in Fig. 1(a) by looking at the rolled up shape of PSi membranes and this is the main limit to fabricate single layer thick samples (multilayers have a greater mechanical strength probably

due to a partial compensating effect of the low porosity layers). Still, all the Raman analysis performed so far does not separate the different roles played by the nanostructures (where phonon quantization is the reason of the Raman red shift and broadening) from that of the mechanical stress (which is not related to quantum effects and acts on macroscopic length).

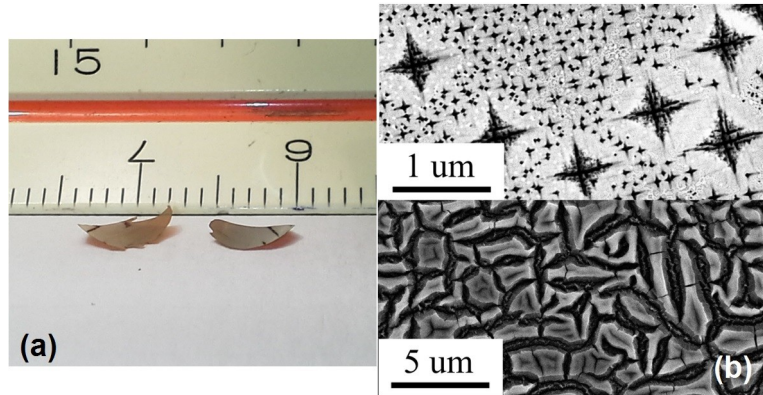


Fig. 1. (a) Photograph of released FSMs which are bent by the mechanical stress accumulated during their etching. The surface in contact with the table is the concave side. (b) Defects on the porous silicon surface: (top) larger pores decorate the surface of surface of a free standing PSi membrane etched in n + silicon. The anisotropy of the etching is clearly underlined by the star shaped pores which indicate the $\{110\}$ lattice directions (scale bar $1\mu\text{m}$). (bottom) Top surface of a p + sample. The dark grooves are the result of the collapsing of neighbor pore walls (scale bar $5\mu\text{m}$).

Recently it has been demonstrated that both nanocrystals and mechanically stressed silicon show large nonlinear optical properties [15, 16], thus the knowledge and the mastering of the stress on silicon nanostructures is a fundamental parameter to optimize both their mechanical and optical properties.

In this article we have prepared PSi samples with an optimized structure to underline the difference of these two contributions to the Raman shift. Typical length-scale of pore and pore walls is of the order of 100 nm (thus, too large to show quantum effects [6]) but still the surface of the pores is decorated with Si nanocrystals (Si-NC) and their presence is detected from the typical light emission. An in depth analysis of the samples' porous structure can be found in [17].

We found that the tensile stress accumulated during the etching process by the porous membrane is partially compensated by the presence of the substrate and, in the case of FSMs, released. Furthermore the releasing of the porous layer from the underlying substrate removes the nanocrystals as demonstrated by the disappearance of the PL signal), thus FSMs permit to decouple the quantum and mechanical effects and to obtain a direct and clean measure of the mechanical stress accumulated by the porous layers.

2. Experimental details

Raman spectra were acquired using a LabRam Aramis (from Jobin-Yvon Horiba) using a 632.8 nm HeNe laser as excitation source and either 50x ($2\mu\text{m}$ diameter beamspot size) or 100x ($1\mu\text{m}$ diameter beamspot size) microscope objective in back scattering configuration. The detector is an air cooled CCD (1024 x 256 pixels). The laser power was attenuated, during the spectra acquisition, down to about 0.7 mW in order to minimize the thermal effects (power density was about 10^4 W/cm^2), which is a conservative value to avoid thermal effects as demonstrated by literature [18, 19]. No polarizers have been used and the measurements can be considered as non-polarized, as the informations on the Silicon crystalline direction after detachment of the PSi membrane are lost.

MicroRaman was used to minimize the volume investigated within the membranes and to focus over selected area to avoid the collection from domains containing defects (such as the defective pores and the collapsed area shown in Fig. 1(b)). The importance of the area investigated is generally underestimated in literature: PSi may show several types of defects on its surface and representative areas have to be chosen to collect significant data; moreover, despite the ideal randomness of the pore's distribution, an average over several areas should be performed to assess a proper distribution of nanostructures and mechanical stress.

The total scattered light intensity collected from the surface can be estimated following the treatment presented in [20], considering the absorption coefficient of the silicon at 632.8 nm ($3.3 \times 10^3 \text{ cm}^{-1}$) [21] which gives a penetration of about three microns.

All samples were etched using the same etching conditions: (100) oriented n-Si 0.01 $\Omega \cdot \text{cm}$ was immersed in a solution of HF/H₂O/Ethanol = 25/200/1, current density was kept fixed at 35 mA/cm². For this solution and current density, etch rate was measured to be 21 nm/s. Membranes are detached using a different solution: HF/Ethanol/H₂O₂ = 23.4/150/45 and 70 mA/cm² [22].

3. Discussion

Raman spectra are represented in Fig. 2 for PSL and FSM samples. Results are reported for the convex (top) surface for samples etched between 4 and 30 minutes (i.e. porous layer thickness between 5 and 39 μm , respectively). Each membrane was measured on at least 4 different points.

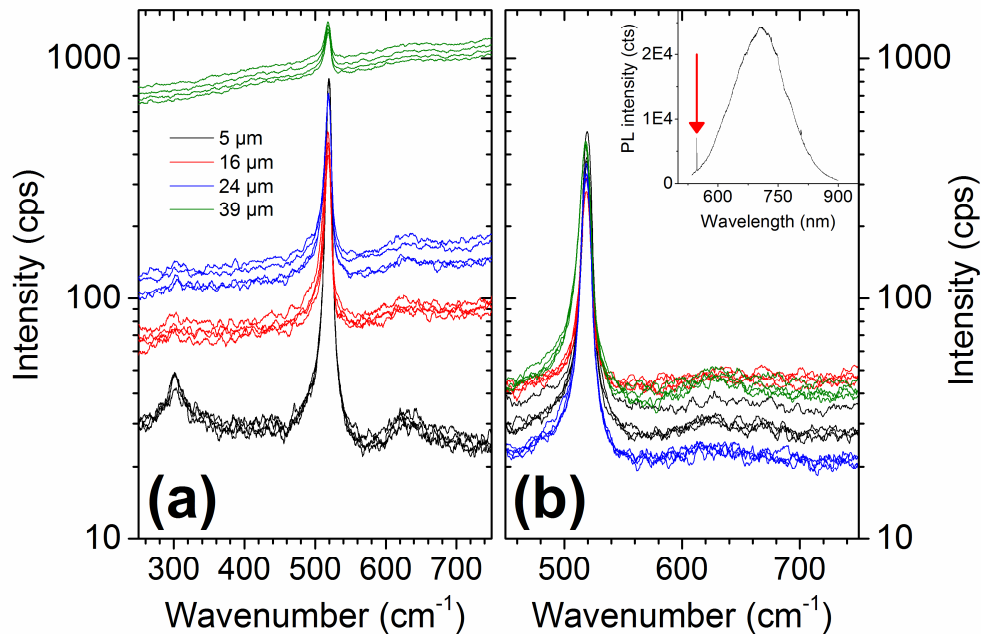


Fig. 2. Raman spectra of (a) PSL and (b) FSM samples. The background below PSLs is related with the appearance of PL signal coming from the smaller nanostructures etched by the direct dissolution of PSi. FSMs show only a negligible increase of the background with etching time. The numbers refer to the thickness of each layer, related to their etching time. Data are smoothed using an Adjacent-averaging method. The inset shows the PL of a PSL, where the red arrow indicates the Raman peak of the silicon.

The Raman lineshape of silicon nanostructures has been investigated using different models. The Fano formula has often been used to fit the spectra because it allows quantifying the asymmetry of the Raman peak as a result of the coupling between the continuum of the Raman virtual states and the phononic band. A recent publication [23] has outlined the limits of this model and the unphysical meaning of corrections that are often needed to fit the experimental data. The authors demonstrated that the original Fano formula can be generalized into a weighted sum of a Fano and a Lorentzian lineshapes, in order to describe asymmetric resonances: The equation number should appear only at the right hand margin of the last line of the equation:

$$F(\varepsilon) = I \left(\eta \frac{(\delta + \varepsilon)^2}{\delta + \varepsilon^2} + \frac{1 - \eta}{1 + \varepsilon^2} \right) \quad (1)$$

The first term within the curly brackets describes the Fano lineshape while the second is the Lorentzian contribution. I is a parameter proportional to the intensity of the Raman peak, η weights the Fano ($\eta = 1$) vs the Lorentzian ($\eta = 0$) contribution to the final lineshape, while δ is a parameter that defines the asymmetry of the peak: $\delta > 0$ indicates a longer peak tail at greater wavenumbers, the opposite for $\delta < 0$. ε is a reduced energy scale. In the following all the spectra were analyzed using this equation. A baseline subtraction has been performed using a modified version of an open source script [24] to remove the strong background due to the PL.

We noticed in Fig. 2 that all Raman peaks showed a slightly long tail on the left side of the lineshape (and confirmed by the always negative value of the δ factor in our simulations) consistent with another literature report [6]. Unfortunately no clear trends were obtained on the values of neither η nor the δ parameter versus the etching time (which is proportional to the sample thickness). This fact is determined mainly by two reasons: the relatively small asymmetry of the peaks is masked by the instrumental noise and the peak shape is determined by the local structure investigated, thus different lineshapes may be recorded at different sampling points. Despite this limitation, the Raman spectra of FSM and PSL show a distinct behavior vs etching time: a broad background signal grows proportionally to the PSL etching time and it is related with the onset of a photoluminescence (PL) signal emitted from Si nanocrystals generated by the lateral dissolution of the pores (see inset Fig. 2(b)). On the other hand FSM samples show only a negligible background: it is likely that the large current burst applied to release the membrane fosters a dissolution of the smaller nanostructure and a correspondingly decrease of the PL.

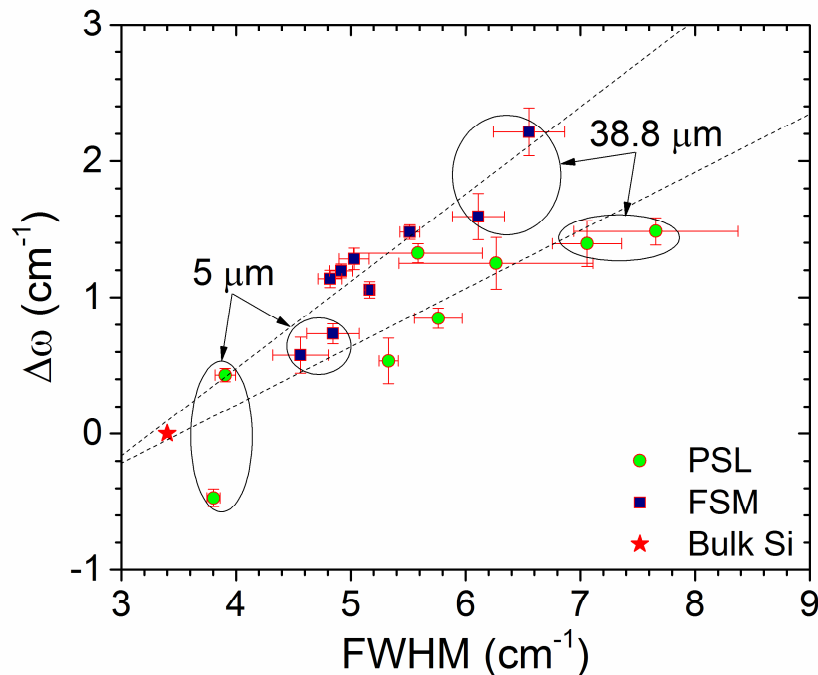


Fig. 3. Raman shift vs FWHM. The shift is calculated by subtracting the wavenumber of the samples to that of the monocrystalline silicon. PSLs show a smaller slope compared to FSMs due to the mechanical constrain of the underlying substrate: once FSM is released from the wafer, it is free to bend and relax the internal stress as demonstrated by the larger shifts. Numbers refer to the thickness of the extrema layers for both PSL and FSM sample sets.

The different evolution of the Raman signal in PSL and FSM samples is apparent also in Fig. 3 by plotting the absolute value of the Raman shift (calculated as $\Delta\omega = \omega_{\text{crystSi}} - \omega_{\text{PSi}}$) versus its FWHM. Error bars are obtained from the average over two sets of samples. We found that, accordingly to the literature [7, 25], PSi is under tensile stress because of the positive value of the shift. In fact, as expected both linear extrapolations of the sets of data point towards the null Raman shift of the crystalline silicon (represented as a red star in Fig. 3).

It is important to note that FSMs show the largest $\Delta\omega$ and the steepest dependence (1.3 vs 0.9) of it vs FWHM. These facts indicate that the substrate partially compensates the tensile stress accumulated by the membranes during their fabrication.

Contrary to the conclusions traced in [12], the statistics done on several measured areas show that the standard deviation on the FWHM in the case of PSL is almost twice as wide as in the case of FSM (1.9 vs 1.0 cm^{-1}). We believe this fact to be due to the dissolution of the smaller, optically active nanostructures during the releasing of the FSM, as confirmed also by the removal of the PL background in Fig. 2. In fact, as explained in [26], because of the shape of the phonon dispersion bands, quantum effects tend to red shift and broaden the Raman lineshape.

Unfortunately the spread of the experimental data, together with the small Raman shift analysed, do not permit to extract more quantitative information about the mechanical state of the PSi layer. Only a weak trend appears for both FWHM and Raman position vs sample thickness, as shown in Fig. 4.

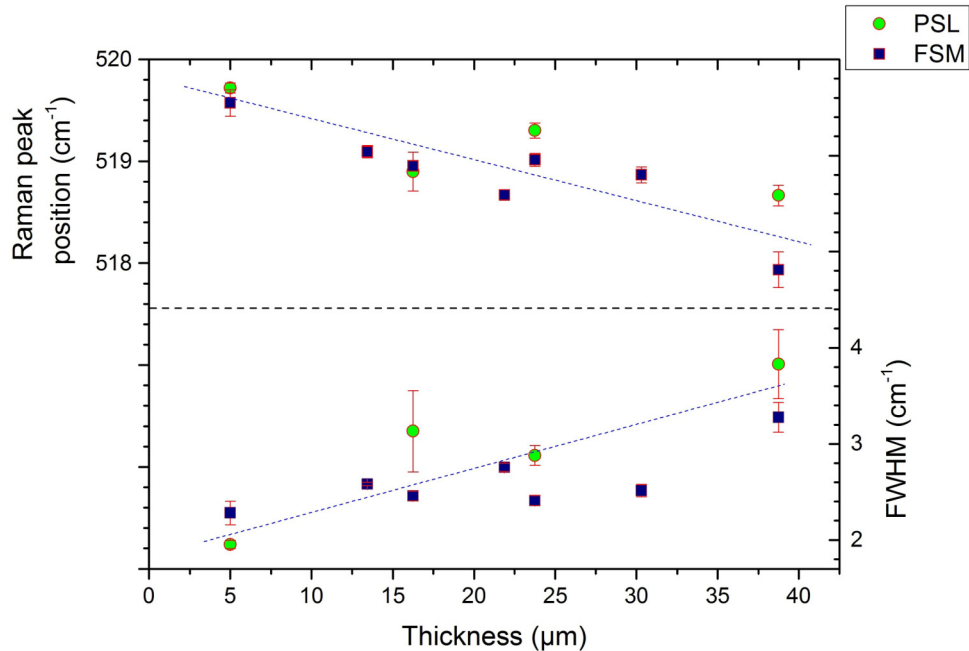


Fig. 4. FWHM and Raman shift vs membrane thickness. The shift is calculated by subtracting the wavenumber of the samples to that of the monocrystalline silicon. Dotted lines are drawn as a guide for the eyes.

This weak correlation is due to the poor control over the macroscopic bending of the FSMs. In fact, even if we tried to obtain rounded shaped FSMs, small shape variations and edge effects induce preferentially bending directions in the membranes. This is the reason why the structure of the FSMs is generally saddle shaped rather than (the more isotropic) cup shaped. Because of the tensorial nature of the stress, this macroscopic bending affects the Raman peak position irrespectively from the crystalline orientation of the Si substrate. In this case, the Raman shift becomes a convolution of a component due to the mechanical stress of the PSi and one linked to the direction in which the FSM macroscopically bends. Nevertheless, albeit being scattered, the data set shows two interesting trends:

1. both the sets (PSL and FSM) lie on a linear trend, rather than fitting the nonlinear function typically reported for this range of $\Delta\omega$ and FWHM [16]. This fact suggests that, at least for the type of samples investigated here, the Raman shift is determined by the mechanical stress, rather than from phonon confinement effects. Thus both $\Delta\omega$ and FWHM increases linearly with sample thickness, supporting the experimental evidence of the fragility of thick FSM;
2. The FSM's data set is contained within a narrower range and it is systematically shifted to higher wavenumbers. This fact supports the idea that quantum effects are negligible in FSMs because both redshifts and spectral broadening due to quantum effects are reduced.

Two other sets of identical FSMs were prepared and used to investigate the differences among the concave and convex surfaces of the detached membranes. Results are reported in Fig. 5. The two symbols refer to the two sets of samples fabricated to check the process reproducibility. Each error bar represents the average of four independent measurements performed on the same sample near the center of the FSM.

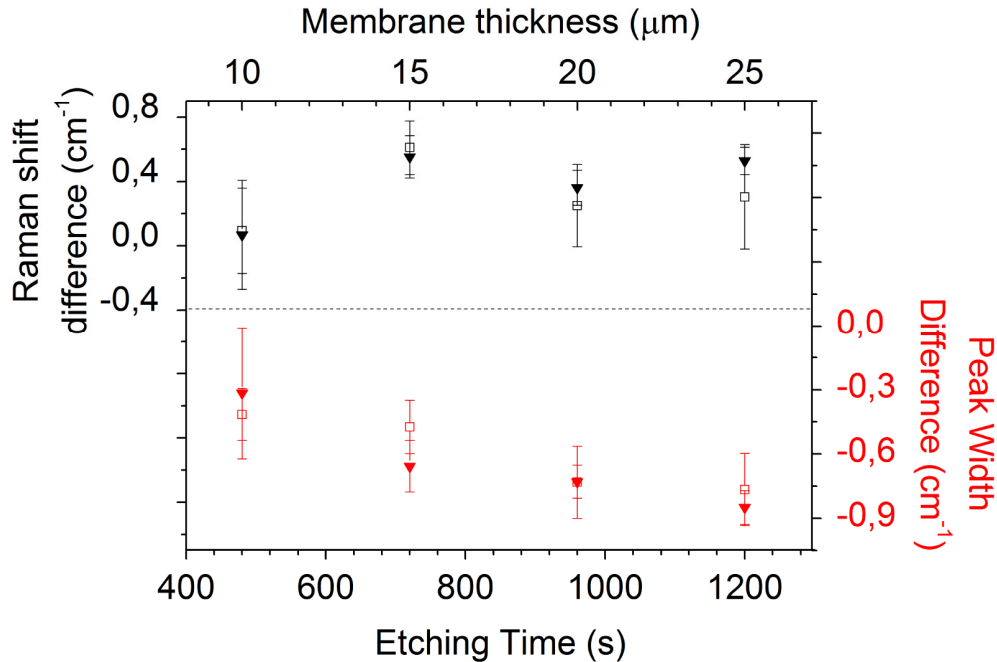


Fig. 5. Differences between concave and convex surfaces of FSMs. Top half of the graph reports the difference of the width of the Raman peaks on the two surfaces (calculated as: concave - convex). The bottom half reports the peak width difference. The two symbols refer to the two sets of samples fabricated.

The graph reports the differences among the values measured on the concave and on the convex surface. The difference in the Raman shift's shift (calculated as $\Delta\omega = \Delta\omega_{\text{concave}} - \Delta\omega_{\text{convex}}$) is rather small and fluctuates vs etching time. This demonstrates that the mechanical stress is relaxed after releasing the porous layer and that there are no differences in the mechanical states of the two surfaces. On the other hand, the peak width difference (calculated as $\Delta\lambda = \Delta\lambda_{\text{concave}} - \Delta\lambda_{\text{convex}}$) shows a more pronounced trend vs etching time. This fact suggests that the size distributions of the PSi skeleton on the two surfaces are different and, in particular, the convex surface has a broader size distribution of silicon nanostructures. This is compatible with a larger concentration of Si nanocrystals created by the chemical etching.

4. Conclusion

In this article we have demonstrated that porous silicon layers accumulate a tensile stress during the etching process, which is partially compensated by the presence of the substrate. In the case of FSMs, this stress is released as demonstrated by the macroscopic bending of the membranes. As the values extracted from Raman peaks measured on PSL are averaged by the tensile stress of the porous layer and the compensating effect of the substrate, the analysis of FSMs are essential for studying stress in porous materials. The results from this study give a clear description of the Raman properties of silicon nanostructures and can serve as a starting point to fabricate samples with optimized mechanical and optical properties.

Acknowledgments

This work was partially supported the Italian Ministry of University and Research through the "Futuro in Ricerca" project RBFR12001G - NEMATIC.